How to Cite: Minaeva, V.A., Karaush-Karmazin, N.N., Panchenko, O.O., Chernyk, M.V., Simokaitiene, J., Volyniuk, D.Yu., Grazulevicius, J.V., Minaev, B.F., & Reshetnyak, O.V. (2023). Structure and Spectral Properties of Thianthrene and Its Benzoyl-Containing Derivatives. *Eurasian Journal of Chemistry, 111(3), 89-103*. https://doi.org/10.31489/2959-0663/3-23-7

Article

Received: 19 May 2023 | Revised: 22 June 2023 |
Accepted: 27 June 2023 | Published online: 01 August 2023

UDC 544.522

https://doi.org/10.31489/2959-0663/3-23-7

Valentina A. Minaeva[1], Nataliya N. Karaush-Karmazin[1*], Olexandr O. Panchenko[1], Maryana V. Chernyk[1], Jurate Simokaitiene[2], Dmytro Yu. Volyniuk[2], Juozas V. Grazulevicius[2], Boris F. Minaev[1, 3*], Oleksandr V. Reshetnyak[4]

[1]*Department of Chemistry and Nanomaterials Science, Bohdan Khmelnytsky National University, Cherkasy, Ukraine;*
[2]*Department of Polymer Chemistry and Technology, Kaunas University of Technology, Kaunas, Lithuania;*
[3]*Department of Physics and Astronomy, Uppsala University, Uppsala, Sweden;*
[4]*Department of Physical and Colloid Chemistry, Ivan Franko National University of Lviv, Lviv, Ukraine*
*(*Corresponding authors' e-mail: karaush22@ukr.net; bfmin43@ukr.net)*

Structure and Spectral Properties of Thianthrene and Its Benzoyl-Containing Derivatives

The IR absorption spectra of the recently synthesized series of benzoyl-containing thianthrene derivatives were studied in the context of their structural identification. Geometry optimization of the ground singlet state by density functional theory (DFT) calculations with the gradient and Hessian search were performed for thianthrene molecule in the framework of the C_{2v} symmetry restriction. The excited singlet and triplet states of thianthrene were found to be distorted along the b_{3u} vibrational mode of the D_{2h} point group, as well as the ground state, which leads to the non-planar batterfly-like structure (C_{2v}). But the excited states require additional symmetry reduction; they are closer to planarity but have no symmetry elements. Optimized ground states structure for the thianthrene-benzoyle molecule and its four derivatives with fluoro-substituents and different substitution positions were analyzed through complete assignment of all their vibrational modes and comparison with experimental infrared absorption spectra. A good agreement between experimental data and DFT calculated IR spectra provides additional structural support to results of the X-ray diffraction analysis of all synthesized compounds. The Hirshfeld surfaces analysis of the crystalline 3-fluorobenzoylthianthrene (**T3F**) was performed in order to analyze intermolecular interactions in **T3F** crystal. It indicates the presence of weak CH…F, CH…S and CH…O intermolecular contacts, stabilizing the crystal structure of **T3F**. The CH…O interactions appear in the IR spectrum of **T3F** crystal as two vibrational modes with frequencies 3084 and 3078 cm^{-1}. The intermolecular interactions CH…F and CH…S do not affect the IR spectrum of **T3F**.

Keywords: thianthrene, benzoylthianthrene, DFT calculations; B3LYP/6-31 G(d, p), IR spectra; X-ray analysis, Hirshfeld surface analysis.

Introduction

Organic dyes containing π-conjugated donor (D) and acceptor (A) moieties, which are connected through effective π-bonds, have attracted considerable attention in modern optoelectronic technologies. In addition to the extended π-conjugated chain, such organic luminophores must satisfy many other requirements, including thermal and chemical stability, high external quantum efficiency, correct redox parameters, and good electron-hole transport characteristics. The thianthrene molecule and its derivatives are interesting luminophores for modern OLED technology due to the high yield of triplet excited states and the ability to create thermally activated delayed fluorescence (TADF) [1].

Thianthrene is the anthracene heterocyclic analog with two sulfur atoms substituents at the 9,10-positions (Fig. 1). Its form consists of two benzene rings disposed into two planes intersecting along the S-S axis at a dihedral angle of 128° [1]. Strong inclination of these two planes and the extended π-electronic conjugation system with peculiar lone pairs at sulfur atoms provide interesting chemical, photophysical and electrochemical properties of thianthrene [2]. The bent, non-aromatic structure of the central dithiine ring leads to the strongly pronounced and expressed electron-donor properties of thianthrene, its stable cation and dication species. While the chemistry and electrochemistry of thianthrene are well studied, its luminescence and photophysical constants have not been propery investigated [1–3]. In particular, Arena et al. [1] studied phosphorescence of the thianthrene molecular crystals accompanied by semiempirical calculation of excited states with vertical excitations, but not many studies of its numerous derivatives were published [1, 2].

Recently synthesized thianthrene-benzoyle derivatives with different halogen substituents and substitution positions have been shown as efficient room temperature phosphorescent emitters with large (>90 %) or moderate phosphorescence contribution to the total photoluminescence and electroluminescence [3]. The X-ray diffraction (XRD) analysis of few synthesized compounds does not afford us to distinguish two types of fluoro-substituted isomers; namely (2-fluorophenyl)(thianthren-2-yl)methanone (**T2F)** and (6-fluorophenyl)(thianthren-2-yl)methanone **(T6F)** benzoyl-thianthrene derivatives without additional study. To do this, we performed IR absorption measurements and DFT calculations of all vibrational modes of four thianthrene-benzoyle derivatives. Comparison of intensity and frequency of experimental and theoretical IR absorption bands permits us to ensure all structural parameters of new synthesized compounds.

We also performed full interpretation of the thianthrene IR spectrum on the basis of DFT calculation of all 60 normal vibrations. The knowledge of the quite accurate calculated thianthrene force field in the ground state helps us to predict the first excited states structure for the singlet (S) and triplet (T) state manifolds. To do this we applied the pseud-Jahn-Teller effect theory [4] and ideology developed by I.B. Bersuker. First, we shall consider the IR spectra problems and then we shall use and illustrate the vibronic perturbation analysis of the pseudo-JT effect [4, 5] comparing the parent anthracene and relative thianthrene molecules in order to explain the ground and excited states of these two particles.

Computational Details

To analyze IR spectra of thiantrene and its derivatives, it is necessary first to carry out quantum chemical calculations of molecular structure of these compounds by optimizing the geometry. The structures of nuclear positions in the studied molecules were optimized by the electronic density calculation at the DFT level using the B3LYP/6-31 G(d, p) method [6–8] based on the initial molecular geometries obtained by the self-consistent field semiempirical PM3 approach [9, 10]. The optimization of the 3-fluorobenzoylthianthrene (**T3F**) molecule was carried out on the basis of the X-ray diffraction analysis data [11]. On the basis of the optimized geometry the theoretical IR spectra of molecules the studied compounds were calculated and analyzed. Vibrational frequencies, wave numbers with the corresponding IR intensities were evaluated in the framework of the same DFT method through the gradients of total energy, dipole moments and force constants calculations. All frequencies of normal vibrations found to be real, which indicates the achievement of a true minimum of the potential energy hypersurface. The best fitting between the experimental and calculated infrared spectra can be achieved implementing three various scale factors for the different types of vibrations: we use 0.950 scaling parameter for the high frequency region of the C–H stretching modes, 0.97 — for C=C stretching vibrations and 0.98 — for the rest of the IR spectrum; that is mostly the CH bending in-plane and out-of-plane vibrations, ring deformations modes. The scale factors were estimated as the ratio of the experimentally observed and DFT-calculated frequencies averaged for all IR bands in the particular region of the spectra. It should be noted that similar scale factors are often used in other studies for the corresponding IR spectral parts [12].

The finally predicted IR spectra of the studied molecules were produced by the GaussView 6.0 software [13] using the chosen half-width of 10 cm^{-1} and the Lorenzian distribution function. The qualitative vibrational assignment of all normal modes in terms of the natural coordinates were achieved with the help of animation program by the Chemcraft code [14], which provides a visual presentation of the calculated vibrations. The quantum chemical calculations of electronic structure and vibrational movements were performed by the Gaussian16 program package [15].

The results of IR spectra calculations of the studied molecules were compared with experimental data for the synthesized compounds [3].

The Bruker Vertex 70 infrared spectrometer (Vertex 70, Bruker Corporation, Germany) with the samples in the form of KBr pellets was used to record FTIR spectra.

The Hirschfeld surface of the studied crystal of the compound **T3F** was calculated using Crystal Explorer 17.5 software with a very high resolution [16, 17].

Results and Discussion

Structural features and IR spectra of thianthrene and benzoylthianthrene

The crystal and molecular structure of thianthrene was analysed by X-ray diffraction [18]. The chemical structure of thianthrene is shown in Figure 1.

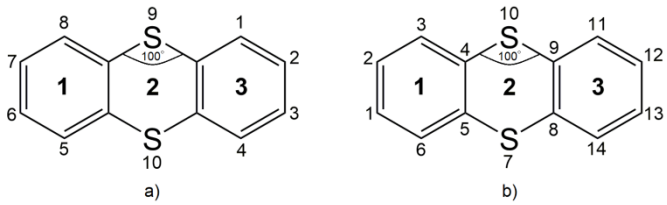

a — chemical numbering of atoms; *b* — numbering of atoms is set by the Gaussian program

Figure 1. Chemical structure of thianthrene

The molecule was found to be folded in respect to the S···S axis so that two benzene rings lie in two planes at an angle of 128°, the bending CSC valence angle is 100° and C–S bond lengths is 1.76±0.01 Å [18].

Chemical structures of benzoylthianthrene and its fluoro-substituted derivatives are shown in Figure 2.

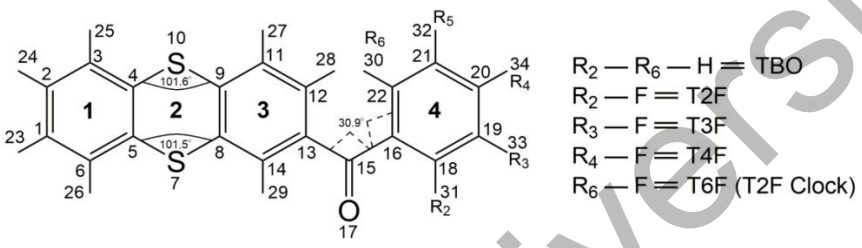

TBO — phenyl(thianthren-2-yl)methanone or benzoylthianthrene; **T2F** — (2-fluorophenyl)(thianthren-2-yl)methanone or 2-fluorobenzoylthianthrene (counter clockwise orientation); **T3F** — (3-fluorophenyl)(thianthren-2-yl)methanone or 3-fluorobenzoylthianthrene; **T4F** — (4-fluorophenyl)(thianthren-2-yl)methanone or 4-fluorobenzoylthianthrene; **T6F** — (6-fluorophenyl)(thianthren-2-yl)methanone or 6-fluorobenzoylthianthrene or **T2F** clock-wise orientation

Figure 2. Chemical structures of benzoylthianthrene and its fluoro-derivatives: the abbreviated names of fluoro-substituted benzoylthianthrenes are given based on the counterclockwise orientation of the substituent on the phenyl ring. The arbitrary atomic numbering generated by the computer program; the same numbers are used for all other fluoro-derivatives for the sake of comparisons

The DFT optimized molecular structures for thianthrene and benzoylthianthrene (**TBO**) are shown in Figures 3 and 4, respectively. Numbering of atoms is set by the program and used in this paper for all other molecules

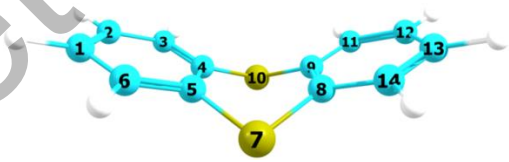

Figure 3. The optimized structure of the thianthrene molecule

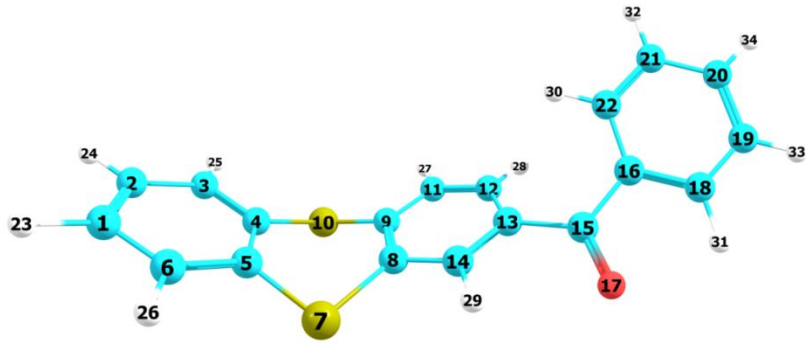

Figure 4. The optimized structure of the benzoylthianthrene (**TBO**) molecule

The calculated atomic charges for all studied molecules are presented in Table; the structural parameters (bond lengths (Å) and angles (deg)) for the thianthrene and **TBO** molecules are given in Table S1 **Supplementary Materials**.

T a b l e

Calculated atomic charges (according to Mulliken) for thianthrene and its benzoyl derivatives in the electron charge units

Atom	Thianthrene	**TBO**	**T2F**	**T3F**	**T4F**	**T6F** (**T2F**, clock wise)
C1	–0.080	–0.079	–0.079	–0.079	–0.079	–0.079
C2	–0.080	–0.080	–0.080	–0.080	–0.080	–0.080
C3	–0.091	–0.090	–0.090	–0.090	–0.090	–0.090
C4	–0.107	–0.110	–0.111	–0.111	–0.111	–0.110
C5	–0.107	–0.108	–0.109	–0.109	–0.109	–0.108
C6	–0.091	–0.091	–0.091	–0.091	–0.091	–0.091
S7	0.157	0.173	0.175	0.174	0.174	0.172
C8	–0.107	–0.117	–0.117	–0.118	–0.118	–0.118
C9	–0. 107	–0.099	–0.099	–0.099	–0.099	–0.098
S10	0.157	0.169	0.171	0.170	0.170	0.169
C11	–0.091	–0.103	–0.102	–0.103	–0.102	–0.105
C12	–0.080	–0.108	–0.109	–0.107	–0.109	–0.109
C13	0.080	0.044	0.044	0.044	0.044	0.057
C14	–0.091	–0.098	–0.100	–0.098	–0.098	–0.099
C15	–	0.329	0.346	0.333	0.330	0.339
C16	–	0.041	–0.037	0.035	0.039	–0.024
O17	–	–0.464	–0.447	–0.460	–0.465	–0.458
C18	–	–0.090	0.341	–0.146	–0.092	–0.092
C19	–	–0.092	–0.138	0.351	–0.143	–0.090
C20	–	–0.075	–0.079	–0.127	0.364	–0.080
C21	–	–0.094	–0.090–	–0.096	–0.147	–0.136
C22	–	–0.116	–0.107	–0.115	–0.117	0.320
H28	0.094	0.109	0.109	0.109	0.108	0.101
H29	0.105	0.131	0.135	0.132	0.132	0.133
H30	–	0.103	0.108	0.106	0.111	–0.287 (F)
H31	–	0.116	–0.272 (F)	0.130	0.125	0.120
H32	–	0.093	0.096	0.102	0.110	0.109
H33	–	0.095	0.109	–0.293 (F)	0.112	0.098
H34	–	0.094	0.101	0.110	–0.289 (F)	0.102

As can be seen from Table S1, the calculated bond angles CSC and bond lengths C–S for thianthrene are close to the experimental values [18]. The calculated C=C bond lengths in thianthrene and benzoylthianthrene are in the range of 1.394÷1.404 Å, which are typical for aromatic C=C bonds. The addition of a benzoyl moiety into the benzene ring number **3** enriches the electron density on the carbon atoms of this ring and pulls the electron density from the sulfur atoms (increases the positive charge) (Table). The calculated dipole moments of the thianthrene and **TBO** molecules are equal 1.6472 and 3.8659 D, respectively.

The benzoyl moiety provides structural distortions in the benzene rings of thiantrene; it mostly affects the length of C=C bonds within the benzene ring number **3** (changes are up to 0.008 Å), the bond angles (up to 1°) and the dihedral angles (changes up to 1.8°) (Table S1). These changes are also observed in the dithiine moiety (thianthrene ring number **2**), but to a less extent. The noted changes should affect the vibration frequencies and absorption intensities in IR spectra of these compounds. Twisting is observed between the thianthrene and benzoyl groups (Fig. 4), the torsion angle C13-C15-C16-C22 is 30.87° (Table S1).

On the background of the gradient derivatives (Hessian) for the optimized geometry the theoretical IR spectra of the studied molecules were calculated and analyzed; the normal vibration frequencies and their IR intensity for the thianthrene and **TBO** molecules are presented in Table S2 and Table S3, respectively. Theoretically predicted IR spectra of both molecules are compared with experimental results of thianthrene [19] and benzoylthianthrene in the Tables S2, S3 and in Figures 5, 6, respectively.

There are 60 normal vibrations in the thianthrene molecule. For the C_{2V} point group symmetry, they can be classified as follows: $15A_1$, $15A_2$, $14B_1$ and $16B_2$. According to the IR vibrational selection rules only A_1, B_1 and B_2 vibrations are allowed in the IR spectrum. All vibrational modes in the thianthrene molecule IR spectrum are presented and assigned in Table S2. Figure S5 illustrates the high-frequency IR absorption region of the thianthrene and **TBO** molecules, Figure S6 shows the finger print parts of IR spectra of those molecules.

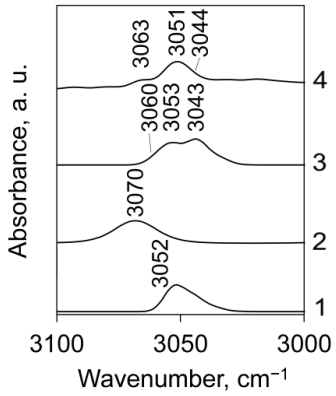

Curve 1 — calculated IR spectrum for thianthrene;
curve 2 — experimental IR spectrum for solid-state thianthrene sample of the studied compound [19];
curve 3 — calculated IR spectrum for the **TBO** molecule;
curve 4 — experimental IR spectrum for the solid-state **TBO** sample

Figure 5. IR spectra of thianthrene and **TBO** in the high-frequency range (3100–3000 cm^{-1})

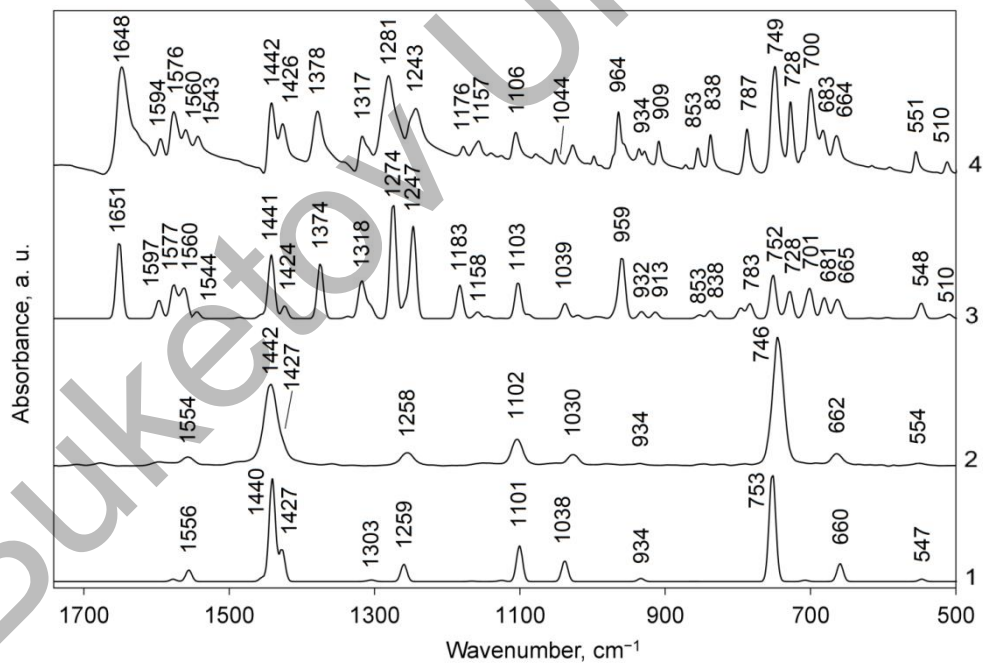

Curve 1 — calculated IR spectrum for the thianthrene molecule;
curve 2 — experimental IR spectrum for the solid-state thianthrene sample [19];
curve 3 — calculated IR spectrum for the **TBO** molecule;
curve 4 — experimental IR spectrum for the solid-state **TBO** sample

Figure 6. IR spectra of thianthrene and **TBO** in the 1700–500 cm^{-1} range

According to the characteristic group frequencies analysis [20], the C–H stretching vibrations in aromatic compounds can be found in the range 3080–3030 cm^{-1}, the CH bending in-plane deformation modes — in the

range 1225–950 cm^{-1} and CH bending out-of-plane deformation vibrations — below 900 cm^{-1}. The IR absorption bands of the aromatic C=C stretching vibrations are usually observed in the region 1650–1430 cm^{-1}. The assignment of all normal modes with the help of animation program of the Chemcraft code [21], which provides a visual presentation of the calculated vibrations, indicates that in the thianthrene IR spectrum the C–H stretching vibrations should be observed in the range 3053–3028 cm^{-1} (calc.: 3052 cm^{-1}, exp.: 3070 cm^{-1}), the planar CH bending deformation — in the range 1259–1101 cm^{-1} (calc.: 1259, 1101 cm^{-1}, exp.: 1258, 1102 cm^{-1}), the bending out-of-plane deformation vibrations — 970–750 cm^{-1} (calc.: 934, 753 cm^{-1}, exp.: 934, 746 cm^{-1}), the C=C stretching vibrations of aromatic rings at in the region 1577–1427 cm^{-1} (calc.: 1556, 1440, 1427 cm^{-1}, exp.: 1554, 1442, 1427 cm^{-1}). Most of the bands in the calculated and experimental spectra of thianthrene have a weak absorption intensity (Table S2, Fig. 6, curves 1, 2). The most intense absorption bands in the thianthrene IR spectrum are connected with the out-of-phase asymmetric C=C stretching vibrations (calc.: 1440 cm^{-1}, exp.: 1442 cm^{-1}) and symmetric CH bending out-of-plane vibrations (calc.: 753 cm^{-1}, exp.: 746 cm^{-1}). The C–S stretching and CSC bending modes are mixed with other type of vibrations and contribute to the experimental bands 1443, 1427, 1102, 662 and 554 cm^{-1} (Table S2). We conclude, that the calculated vibration frequencies in the thianthrene molecule are in a good agreement with the experimental spectrum (Table S2, Fig. 6, curves 1, 2).

We attribute the high-frequency shift of the experimental band of stretching C–H vibrations (in the left part of Fig. 5 curve 2) to intermolecular S···H interactions. The noncovalent π–π stacking interactions in the crystal thianthrene structure are unlikely, since the thiantrene molecules are not planar.

The C–H stretching vibrations in the phenyl ring of the benzoyl fragment at 3051 (ν_{92}), 3043 (ν_{90}), 3033 (ν_{87}) cm^{-1} as well as occurring simultaneously C-H modes in the benzene ring (number **3**) at 3060 (ν_{96}) 3059 (ν_{95}) cm^{-1} (Table S3) change the shape of the spectral curve in the high-frequency region of the IR spectrum of **TBO** (Fig. 5, curves 3, 4) compared to thiantrene. The ring number **3** associated with the benzoyl fragment provides total distortion of the **TBO** spectrum (Fig. 5, curves 3, 4).

The addition of the benzoyl moiety to the benzene ring (number **3**) enriches the finger-print IR spectrum with strong absorption bands of C=O stretching vibration (calc.: 1651 cm^{-1}, ν_{84}, exp.: 1648 cm^{-1}, Fug. 6). There are asymmetric C=C stretching vibrations in the benzene ring (number **3**) (calc.: 1374 cm^{-1}, ν_{72}, exp.: 1378 cm^{-1}), asymmetric =C–C(O)–C= stretching vibrations (calc.: 1274 cm^{-1}, ν_{67}, and 1247 cm^{-1}, ν_{65}, exp.: 1281 and 1243 cm^{-1}), asymmetric ring deformation. in-plane, in the aromatic rings number **3** and **4** (calc.: 959 cm^{-1}, ν_{47}, exp.: 964 cm^{-1}, Table S2, Fig. 6, curves 3, 4). Strong differences between **TBO** and thianthrene IR absorption is also determined by the normal vibrations ν_{83}, ν_{70}, ν_{64}, ν_{44}, ν_{34}, ν_{33}, with frequencies 1597, 1318, 1183, 932, 707, 701 cm^{-1} in the phenyl ring of the benzoyl fragment as well as the normal vibrations ν_{41}, ν_{40}, ν_{39}, ν_{38}, ν_{35}, ν_{31} and ν_{30}, with calculated frequencies 853, 838, 796, 783, 728, 681 and 665 cm^{-1} occurring simultaneously in the phenyl ring of the benzoyl fragment and in the benzene ring (number **3**) associated with the benzoyl fragment form in the IR spectrum absorption bands with medium and medium-to-weak intensities (Fig. 6, curves 3, 4). The assignment of these bands is given in Table S3. Thus, a change in the charges on atoms, bond lengths, and bond angles in the benzene ring of thianthrene (ring number 3) upon addition of a benzoyl fragment leads to a change in vibration frequencies and their intensities, and to the appearance of new vibrations (Fig. 6).

The effect of the fluoro-substituent in the benzoyl fragment on the IR spectrum of benzoylthianthrenes

Due to the fact that the phenyl ring in the **TBO** molecule is not conjugated with the thiantrene fragment, the substitution of a hydrogen atom by a fluorine atom in the phenyl ring does not significantly affect the electron density redistribution in the thiantrene fragment, but it has a significant effect on the electronic properties of the phenyl ring itself. Because of the strongly electron-withdrawing nature of the fluorine atom, a slight polarization of the benzene ring of the thianthrene fragment associated with the benzoyl fragment and the carbonyl link through the hyperconjugation system between this ring and the corresponding benzoyl substituent is observed. Thus, in the molecules of **T2F** counter clock-wise orientation and **T2F** clock-wise orientation, a decrease in the electron density is observed on the C15 and O17 atoms, and in the **T2F** clock-wise orientation molecule and on the C13 atom (Table).

The substitution of hydrogen atom by fluorine atom in phenyl ring also does not cause a visible change in bond lengths and bond angles within the thiantrene fragment, but affects the length of C=C bonds within the phenyl group (changes are up to 0.006 Å), bond angles (up to 3°) and the dihedral angles change significantly (up to 16°) (Table S1). These changes are calculated for molecules **T2F** and **T6F**. The dipole mo-

ments of the **TBO**, **T2F**, **T3F**, **T4F** and **T6F** molecules are equal 3.87, 4.79, 4.66, 3.39, and 3.25 D, respectively. The **T2F** and **T3F** are more polar molecules which agree with the slow cooling of the melting samples.

The noted changes should affect the vibration frequencies and absorption intensities in the IR spectra of these compounds.

The calculated normal vibration frequencies and their intensity in IR spectra of the **T2F** and **T6F** molecules are presented in Tables S4 and S5 of **Supplementary Materials**, respectively. Theoretical predicted IR spectra of both molecules are compared with experimental spectrum of **T2F** compound in Figure 7.

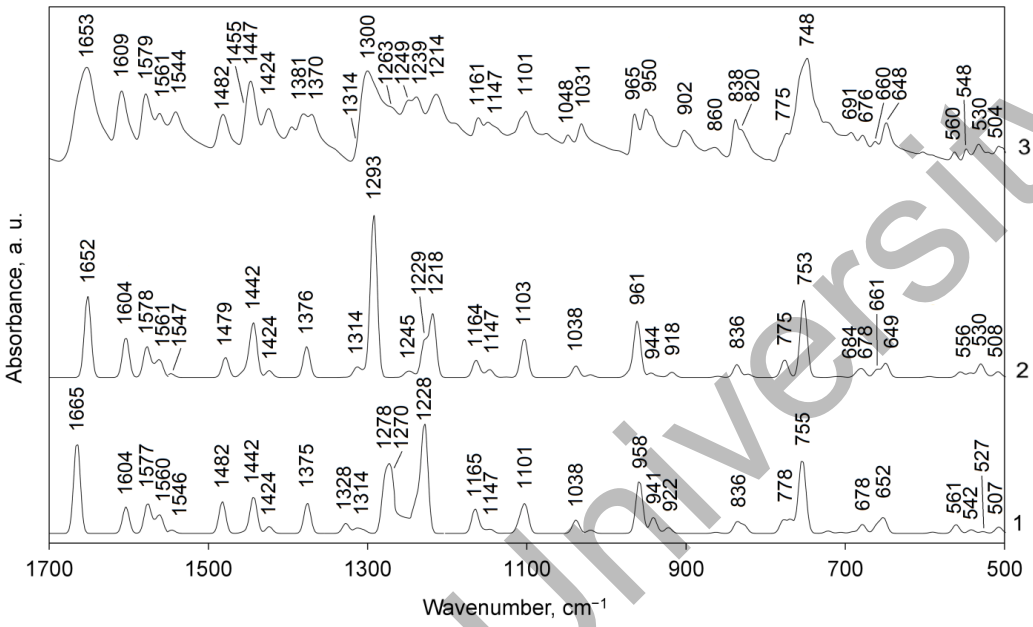

Curve 1 — IR spectrum for the **T2F** molecule calculated in vacuum;
curve 2 — IR spectrum for **T6F** molecule, calculated in vacuum;
curve 3 — experimental IR spectrum for **T2F** compound

Figure 7. Absorption IR spectra of the 2-fluorobenzoylthianthrene derivatives in the 1700–500 cm^{-1} range

Comparison of theoretical IR spectra of both molecules with the experimental spectrum compound **T2F** indicates that calculated IR spectrum of molecule **T2F** clock-wise orientation **(T6F)** fits better the observed IR bands profile. For example, the strong absorption bands C=O stretching vibration at 1652 cm^{-1} in the DFT-calculated IR spectrum of molecule **T6F** coincides with the similar band in the experimental IR spectrum of the **T2F** species (Fig. 7, curve 2 and 3; Table S5, ν_{85}) while in the calculated spectrum of the molecule **T2F** such IR band is shifted by 12 cm^{-1} to the region of high frequencies (Fig. 7, curve 1 and 3; Table S4, ν_{85}, calc.: 1665 cm^{-1}). The calculated frequency 1293 cm^{-1} very strong band asymmetric =C–C(O)–C= stretching vibrations with contribution from C–F stretching vibrations in the IR spectrum of molecule **T6F** (ν_{69}, I = 335 km/mole) close in value to the experimental frequency of 1300 cm^{-1} in the IR spectrum of the **T2F** species while in the calculated spectrum of the molecule **T2F** such IR band but with a lower intensity is formed by two normal vibrations (ν_{69} and ν_{68}) and only in one of them (ν_{69}) there is a contribution from C–F stretching vibrations. It should be noted that all calculated vibrational modes in the IR spectrum of **T6F** in the frequency range 1298–1214 cm^{-1} have a contribution from C–F stretching vibrations, while in the calculated IR spectrum of molecule **T2F** in this frequency range only two modes (ν_{69} and ν_{66}, Table S4) have a contribution from C–F stretching vibrations, which also has an influence on the frequency and intensity of normal vibrations in this region. Based on the calculation of the IR spectrum of the **T6F** molecule, we assign experimental band at 1214 cm^{-1} of the middle intensity (Fig. 7, curve 3) to the =C–C(O)–C= stretching vibrations with contribution from C–F stretching and CH bending in-plane vibrations (calc.: 1218 cm^{-1}). In the IR spectrum of **T2F** molecule this normal vibrations, having lost the contribution of C–F stretching vibrations, formed a strong band shifted towards higher frequencies up to 1228 cm^{-1} (Fig. 7, curve 1, Table S4). These differences can be used to discern the **T2F** and **T6F** isomers with different positions fluorine atom in the phenyl ring.

The total energies of the optimized **T6F** and **T2F** isomers calculated at the B3LYP/6-31G(d, p) level are equal to –1702.1059422 and –1702.1037699 a.u, respectively. Thus, the clock-wise isomer **T2F** is more stable although the energy difference is small, only 5.7 kJ/mol.

Thus, comparative analysis of the calculated IR spectra of two isomers **T6F** and **T2F** affords us to conclude finally that the experimental spectrum of **T2F** compound belongs to the **T6F** compound, where the fluorine substituent is in the position 2 clock-wise orientation of the aromatic ring, therefore, the synthesized **T2F** compound will be referred to as **T6F** (or **T2F** clock-wise orientation).

The calculated normal vibration frequencies and their intensity in IR of the **3F** and **4F** molecules are presented in Tables S6 and S7 of **Supplementary Materials**, respectively, and compared with experimental spectra of these compounds.

For ease of comparison, the experimental and theoretically predicted IR spectra of benzoylthianthrene and all fluorobenzoylthianthrene derivatives in the 3100–3000 cm^{-1} range are shown in Figures S1 and S2, respectively, and in the 1700–500 cm^{-1} range are shown in Figures 8 and 9, respectively. Assignment of selected bands in the IR absorption spectra for all studied compounds summarized in the Table S8.

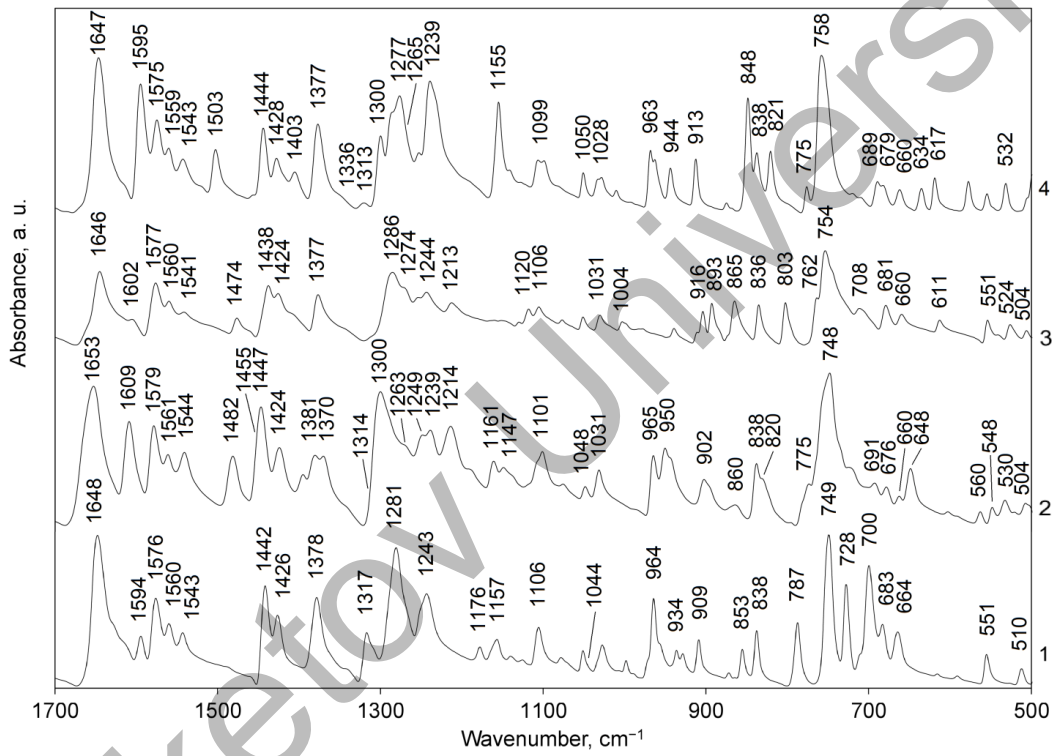

Curve 1 — IR spectrum for **TBO** compound; curve 2 — IR spectrum for **T6F (T2F**clock-wise orientation) compound; curve 3 — IR spectrum for **T3F** compound; curve 4 — IR spectrum for **T4F** compound

Figure 8. Experimental IR spectra of solid-state samples of the studied compounds in the 1700–500 cm^{-1} range

As can be seen in the calculated IR spectra (Fig. 9), the C=O band of the **T2F** isomer is observed at a higher frequency (1665 cm^{-1}, curve 5) compared to the **TBO** molecule (1651 cm^{-1}, curve 1) and **T3F**, **T4F** and **T6F** isomers (1653, 1649, and 1652 cm^{-1}, respectively; curves 3, 4, and 5), which is consistent with a decrease in the C=O bond length (Table S1). The calculated intensity of the C=O normal mode is the highest for **T2F** (191 km/mol, Table S4) compared to 145, 156 and 167 km/mol for the **T3F**, T4F and **T6F** particles (Table S6, S7 and S5). It should be noted that the Mulliken's atomic charges calculated at the O17 atom of the carbonyl group in **T2F** molecule (–0.447*e*) is also different from those for **TBO, T3F**, **T4F** and **T6F** molecules (–0.464, –0.460, –0.465, and –0.468*e*, respectively, Table); thus, the polarity of the bonds could increase but the derivative of dipole moment along displacement could be lower.

The substitution of hydrogen atom by fluorine atom in phenyl ring does not cause a significant change the frequencies of stretching vibrations of C=C bonds in the thianthrene fragment and their IR intensities (Table S8). However, if vibrations of C=C bonds occur in the phenyl ring of the benzoyl fragment, then the IR frequencies and intensity change. So, the asymmetric C=C stretching vibrations occurring in the phenyl

ring of the **T4F** molecule at 1504 cm^{-1} (exp. 1503 cm^{-1}) appear in the calculated and measured IR spectra of the other fluoro-isomers at lower frequencies and in **T2F** — with higher intensity (Fig. 8, 9). The corresponding IR band in the calculated and measured IR spectra of **TBO** species is not observed, since it is too weak according to our calculations (Table S8, $I_{calc.}$ = 1 km/mol). It should be noted that this calculated mode in the IR spectrum of **T4F** have a contribution from C–F stretching vibrations. The strong band at 1438 cm^{-1} (calc.: 1433 cm^{-1}) in the IR spectrum of **T3F** and the band of weak intensity at 1403 cm^{-1} (calc.: 1406 cm^{-1}) in the IR spectrum of **T4F** also belong to asymmetric C=C stretching vibrations occurring in the phenyl ring.

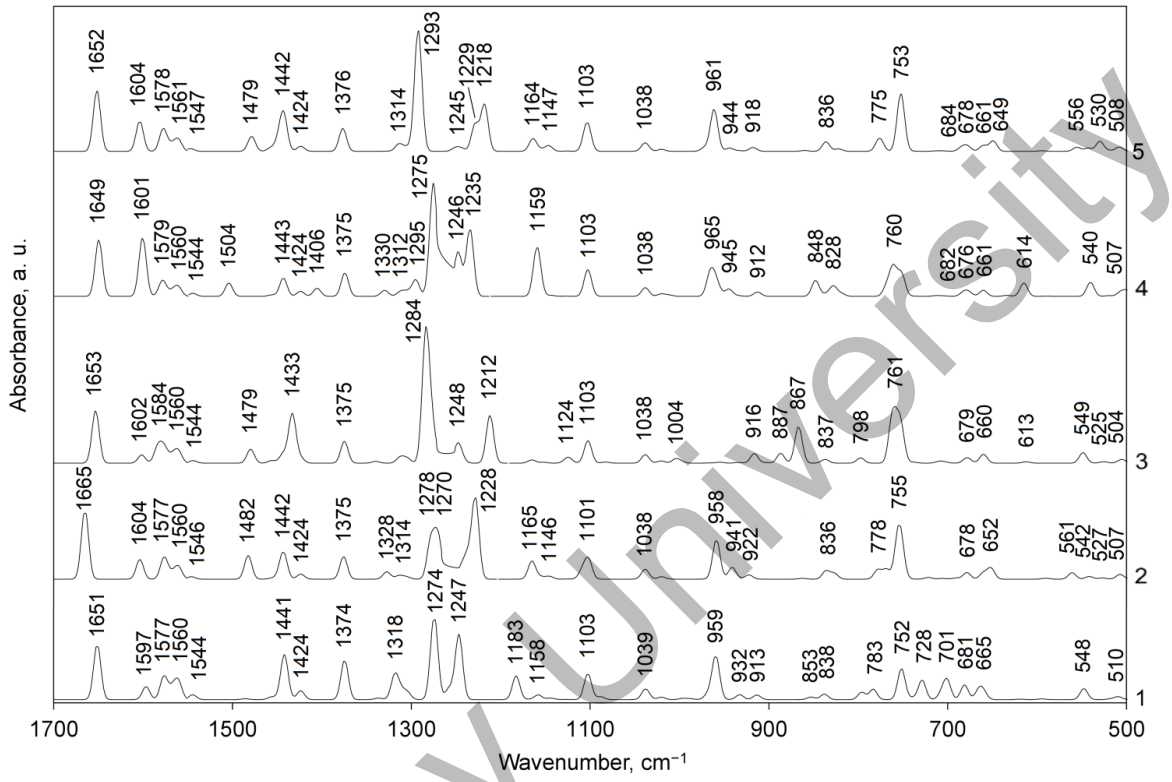

Curve 1 — IR spectrum for **TBO** molecule; curve 2 — IR spectrum for **T2F** molecule; curve 3 — IR spectrum for **T3F** molecule; curve 4 — IR spectrum for **T4F** molecule; curve 5 — IR spectrum for **T6F** molecule

Figure 9. Calculated absorption IR spectra of the benzoylthianthrene and fluorobenzoylthianthrene derivatives in the 1700–500 cm^{-1} range

The weak bands with close frequencies in the calculated and measured IR spectra in the range 1303–1317 cm^{-1} (Fig. 8, 9, Table S8) for all studied compounds are formed by Kekule vibrations in the benzene rings of the thianthrene fragment, which include subsequent alternations of the C=C bonds stretching and compression of large amplitude. In the phenyl ring of the benzoyl moiety the same type of mode occurs at higher frequency and forms in the calculated IR spectra of the **T2F** and **T4F** molecules the weak bands at 1328 and 1330 cm^{-1}. The corresponding bands in the IR spectra of the **TBO**, **T2F** and **T4F** molecules are not observed, since they are too weak according to our calculations. The largest changes in the IR spectra of fluorosubstituted benzoylthianthrenes are observed in the frequency range of 1300–1120 cm^{-1} where asymmetric stretching vibrations of C–C(O)–C bonds of the carbonyl link occur with participation of the C–F bonds stretching and CH groups bending vibrations. We discussed these differences above when comparing the IR spectra of **T2F** and **T6F** compounds. They are also observed for the **T3F** and **T4F** compounds as compared to **T2F**, **T6F** and **TBO** samples (Fig. 8, 9, Table S8).

In the simulated and experimental IR spectra of all studied compounds the weak bands with close frequencies in the range 1099–1106 cm^{-1} (Fig. 8, 9, Table S8) are formed by CH bending vibrations in plane in thiantrene fragment. Asymmetric ring in-plane vibrations in thiantrene fragment are calculated at 1038 and 1041 cm^{-1} but they show the weak absorption intensity according to DFT calculation (Table S8). IR bands below 970 cm^{-1} we assigned to the out-of-plane =CH deformation, and to the out-of-plane ring deformation, in-plane or

out-of-plane vibrations. Many modes have a contribution from the C–F stretching vibrations. In the frequency range of 1000–700 cm^{-1}, substitution of a hydrogen atom by a fluorine atom in the phenyl ring significantly affects not only the IR frequencies and intensities, but also the shape of the vibrational modes. We shall only note the main similarities and differences in this respect (Table S8). Thus; the asymmetric non-planar =CH bending vibrations of the aromatic ring **3** and **4** (in-phase) in the vicinity 960 cm^{-1} in the **TBO**, **T2F**, **T4F** and **T6F** samples form medium IR bands, but the corresponding vibration in **T3F** (calc.: 965 cm^{-1}) provides low calculated intensity (0.5 km/mol) and therefore it is invisible in the **T3F** IR spectrum. The asymmetric in-plane ring deformations in the phenyl moiety and the nearest benzene ring of the thiantrene fragment with a contribution of the C–F stretching vibrations in the vicinity 770 cm^{-1} show the weak absorption intensity (16–18 km/mol); however, in the **T3F** spectrum, this type of vibrations occurs at a much higher frequency (867 cm^{-1}) and shows a higher IR intensity (67 km/mol). The medium bands with close frequencies in the measured IR spectra in the vicinity 838 cm^{-1} belong to =CH out-of-plane deformations with contribution C–F stretching vibrations, however, the calculated intensities are smaller. The strong band in the measured IR spectra **T4F** sample at 848 cm^{-1} (calc. too 848 cm^{-1}) formed by asymmetric out-of-plane =CH bending vibrations in benzene ring (number **3**) of the thiantrene fragment and symmetric vibrations of the same type in the phenyl ring of the benzoyl fragment. The strong bands with close frequencies in the vicinity 750–760 cm^{-1} (Fig. 8, 9) for all the studied compounds are formed by the superposition of three modes symmetric out-of-plane =CH bending vibrations in aromatic rings. IR bands below 710 cm^{-1} we assigned to ring vibrations out-of- plane or symmetric ring deformations in- plane in aromatic rings.

We connect the observed differences with the significant changes in the electronic properties and structural parameters of the phenyl ring depending on the position of the substituent (fluorine atom), as well as with the slight changes in those parameters in the benzene ring **3** of the thiantrene fragment connected with the benzoyl moiety.

The pseudo-Jahn-Teller effect role in the sructural distortion of thiantrene and its derivatives

This scrutinize analysis of the IR spectral differences for the studied thiantrene-benzoyl derivatives afford to clearly distinguish two isomers **T6F** and **T2F** and also to understand photophysical parameters of the whole isomers family obtained from UV-vis absorption and lumineascence studies [3]. Knowing the accurate force field of all studied molecules we can now analyze in details the structure of the thianthrene ancestor molecule in the ground and excited states in order to transfer the similar vibronic perturbation theory to other benzoyl-containing derivatives accounting the pseudo-Jahn–Teller (PJT) effect.

The best approach to solve the problem of the molecular shape prediction should rise the question: *how do electrons influence and control nuclear configurations?* Or how do electronic states deformations affect the nuclear mutual displacements in terms of vibronic perturbation theory? The Jahn–Teller (JT) theorem says that nonlinear polyatomic molecule in the degenerate electronic states is unstable and spontaneously distorts in order to remove the degeneracy [4]. The most important sequence of the JT theorem is the pseudo-JT effect, which considers excited states involvement into vibronic coupling [4, 5]: when two electronic states are not strictly degenerate but are close in energy (pseudo-degenerate), the JT effect is not quenched but only modified, producing similar structural distortions like those caused by the original JT effect. The PJT effect received little attention from the beginning, but a few decades latter Bersuker et al. showed that there is no limitation on the perturbing states energy gap and that the PJT effect is the only source of distortions (instability) of high-symmetry configurations of any polyatomic molecule [4, 5].

If we know the detailed mechanism of the thianthrene distortion from the planar anthracene configuration via the pseudo-JT effect (since one has revealed the vibronically active excited state in this mechanism), we can try to influence the system by means of external perturbations that violate the pseudo-JT-induced B_{3u} condition of thianthrene instability in the ground state. Such perturbation technique could help us to modulate proper excited state properties of various thianthrene derivatives. In principle, there are four possibilities to provide such perturbation treatment: (a) to increase the energy gap between those electronic states which are mixed by the pseudo-Jahn-Teller vibronic coupling (for example, by conjugation with new substituent like benzoyl outside system), (b) to change the symmetry of the vibronically active excited state by adding number of electrons (which could change the parameters of the pseudo-JT effect and the energy gap), (c) to add appropriate substituents that restore the planarity of molecular structure, and (d) by spectroscopic photoexcitation. The method (a) was used in the studies of the mechanism of hemoglobin oxygenation [4, 5] in which the out-of-plane displacement of Fe(II) ion from the hem-porphyrin ring (induced by forces driven by

pseudo JT effect) returns back into the porphyrin plane by oxygenation due to increase of the energy gap from the active state; this illustrates suppressing of the pseudo-JT effect.

The mechanism (b) was demonstrated recently by Bersuker [5] by coordination of two Cl-anions to on-planar (distorted by the PJTE) chair structures of the Si_6Cl_{12} cluster in order to obtain dianion $[Si_6Cl_{14}]_2^-$ with a planar Si_6-ring; here the pseudo-JT effect is suppressed because the empty molecular orbitals of the excited active state in the Si_6-ring became occupied by electrons from two chloride ions [5].

Bersuker et al. [4, 5] have studied numerous manifestations of the pseudo Jahn-Teller (JT) effect in molecular and solid states structure. They considered the influence of heteroatom substitution in series of tricyclic compounds containing 1,2-dithiine and 1,4-dithiine moieties (carbon sulfide C_6S_8, thianthrene, and antracene, their redox products and derivatives) in order to demonstrate the mechanism of suppression and enhancement of the puckering distortions in redox processes and in chemical substitutions.

In the most recent study [5] they demonstrated for the first time the chemical substitution ability to restore the planarity of cyclic compounds. Spectroscopic photo-excitations in this respect have not yet been studied exploring the pseudo-JT effect [4], and we will try to perform such perturbation analysis based on our knowledge of the force field for new derivatives.

Let us compare anthracene and thianthrene molecules in the planar structure of the D_{2h} symmetry. The puckering distortion in respect to the 9-10 positions transforms as the B_{3u} irreducible representation of the D_{2h} point group; thus, only excited states of the B_{3u} symmetry need to be considered in the vibronic perturbation of the ground A_{1g} state of anthracene upon its transformation into thianthrene by the sulfur substitution in 9-10 positions. Our choice of axes (*z*-is perpendicular to the anthracene plane, *x*-the long axis) differs from that in Ref. [5]; thus, their B_{1u} symmetry corresponds to our B_{3u} representation.

Vibronic mixing of the B_{3u} excited singlet state with the ground S_0 state of the A_{1g} symmetry can be calculated accounting geometry distortion along with the B_{3u} vibrational mode. Thus, we can explain this *butterfly-like* distortion in terms of the pseudo JT effect and explain the real non-planar structure of the thianthrene molecule.

It was shown in Ref. [5] that while the thianthrene molecule is bent at the S-S axis, the oxidized thianthrene dication exhibits a planar configuration with the D_{2h} molecular symmetry. The thianthrene highest occupied molecular orbital (HOMO) b_{3u} is getting empty upon oxidation; that is, it becomes the lowest unoccupied molecular orbital (LUMO) in dication. The thianthrene excited state $b_{3u}\rightarrow a_g$ ($^1B_{3u}$) disappears in the dication, as well as the driving force of the puckering distortion [5]. The reason of the PJT effect in the oxidized thianthrene also disappears which leads to the planar dication structure.

Similarly, we have shown that the first excited S_1 state of thianthrene tends to planarization. In the planar structure S_1 state possesses the $^1B_{3g}$ symmetry ($b_{3u}\rightarrow a_u$ excitation). The perturbing state along the puckering b_{3u} mode could be the ^1A_u state associated with the $a_u\rightarrow a_g$ excitation. Such state has a very large energy (6.2 eV) and the distorting PJT effect in the S_1 excited thianthrene is less pronounced than in the ground S_0 state. This vibronic analysis of the b_{3u} puckering distortion is completely supported by TD DFT geometry optimization. The dihedral angle 2-3-4-9 is close to planarity; it changed from 128 to 167° upon excitation. Geometry optimization in the lowest triplet T_1 state with the UB3LYP functional produces larger planarization with additional distortion and strong spin polarization in one phenyl ring. Thus, the thianthrene molecule in the T_1 state has no symmetry elements, which could explain more efficient spin-orbit coupling and enhanced phosphorescence of the thianthrene crystal [1–3].

*Hirshfeld surfaces analysis for the **T3F** crystal*

The nature of the intermolecular contacts stabilizing the crystal structures of the **T3F** and the peculiarities of the influence of these intermolecular interactions on the IR spectrum were explained by the HS analysis. The **T3F** compound crystallizes in the monoclinic ($P2_1/n$) space group. The cell packing and HS of the **T3F** mapped over d_{norm} is presented in Figure 10.

As can be seen in the Hirshfeld d_{norm} surface plot, the crystal structure of **T3F** is stabilized by weak long-ranged CH…F, CH…S and CH…O intermolecular interactions with experimental distances of 2.610 Å, 2.923 Å and 2.827/2.860 Å, respectively, which are indicated as barely visible pale red spots in HS. The shortest contact 2.293 Å in **T3F** crystal belongs to weak H…H intermolecular contacts.

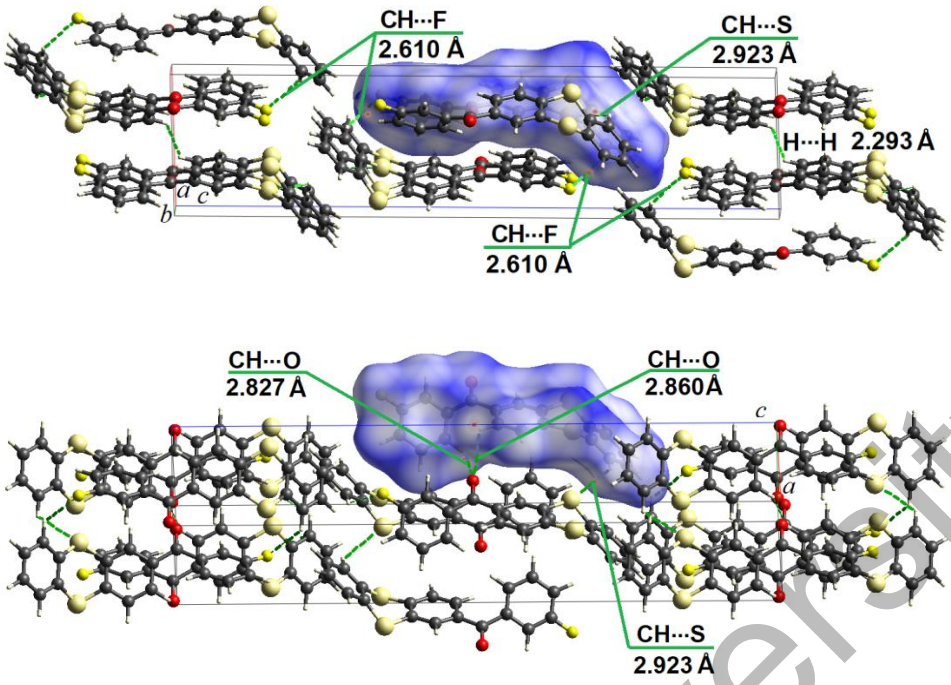

Figure 10. The cell packing and Hirshfeld d_{norm} surface of the intermolecular interactions for **T3F** compound demonstrating CH…F and CH…S interactions (top view) and CH…O interactions (bottom view). Intermolecular interaction is shown by green dashed lines

The study of the manifestation of intermolecular interactions in the IR spectrum of **T3F** was carried out by isolating two dimers (Fig. 11) from the crystal with their further optimization by the B3LYP/6-31G(d, p) method (Fig. S5 in **Supplementary Materials**). This approach has proved to be successful in our recent paper [21–23]. Dimer 1 represents the presence of H…F intermolecular interactions, while dimer 2 displays the shortest H…S and H…O intermolecular interactions. In addition, the CH…S intermolecular interaction between the hydrogen atom of ring I of the thianthrene fragment and the sulfur atom of the neighboring dimer with a distance of 2.923 Å was established (Fig. 10).

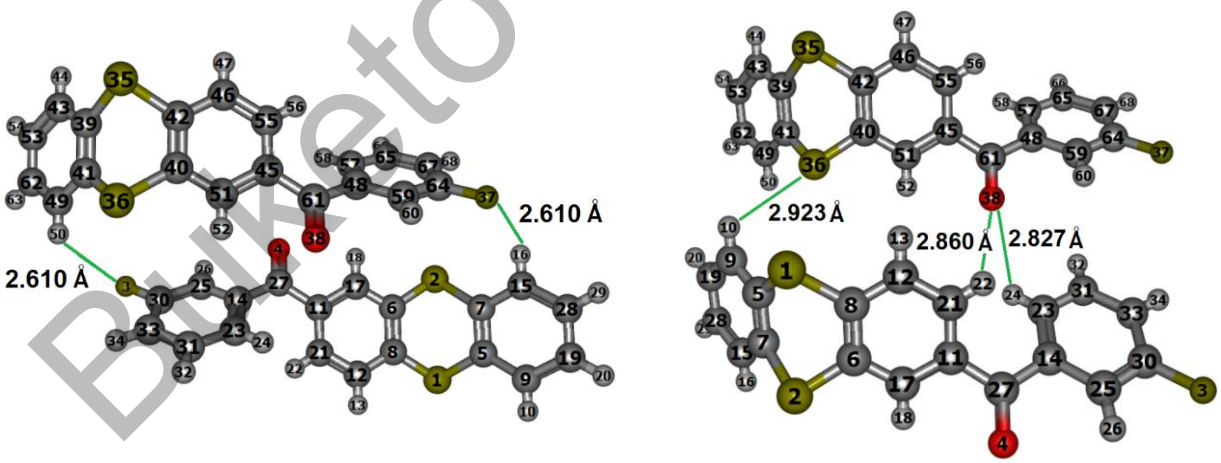

Dimer 1 Dimer 2

Figure 11. The structures of dimers 1 and 2 of **T3F** selected from the X-ray crystal data. Selected experimental intermolecular distances (Å) for the dimers are indicated. The S atoms are 1, 2, 35 and 36, O atoms are 4 and 38, F atoms are 3 and 37. The numbering of atoms in dimers is set by the program and does not coincide with the numbering of atoms in the **T3F** molecule

Theoretically predicted IR spectra of **T3F** molecule and both dimers are compared with experimental results of **T3F** compound in Figures S3 (in the 3100–3300 cm^{-1} range) and S4 (in the 1700–500 cm^{-1} range). Each of the dimers has 184 normal vibrations. Dimer 1 has the C_h symmetry. For the C_h point group sym-

metry, the normal vibrations of the Dimer 1 can be classified as follows: $92A_g$ (gerade) and $92A_u$ (ungerade). According to the IR vibrational selection rules only A_u vibrations are allowed in the IR spectrum. The calculated Dimer 2 has no symmetry; therefore, all normal vibrations in the IR spectrum of dimer 2 are allowed. As can be seen in Figures S3, S4, the experimental IR spectrum of the **T3F** compound and theoretically predicted IR spectra of both **T3F** dimers and molecule are close. The calculated IR intensities of the corresponding IR bands of Dimers 1 and 2 (Figures S3, S4, curves 2, 3) are much higher than those for the molecule (curve 1), since the calculated intensities are almost doubled for two molecules.

Intermolecular interactions H…F and H…S found in Dimer 1, and H…S found in Dimer 2 do not affect the IR spectrum. The intermolecular interactions H…O found in Dimer 2 form two vibrational modes: ν_{198} (=C21–H (**1**)···O (**2**) and=C23–H (**1**)···O (**2**) stretching in-phase) and ν_{197} (the same stretching out-of-phase) in with frequencies 3084 and 3078 cm^{-1}, respectively; however, their calculated intensities are very weak (0.2 and 2 km/mole, respectively) and therefore they do not give visible bands in the IR spectrum of Dimer 2 (Figures S3, curve 3).

Conclusions

The recently synthesized benzoyl-containing thianthrene derivatives were thoroughly studied by DFT optimization of their ground and excited states structures. The thianthrene donor (D) and benzoyl acceptors (A) moieties connected through the strong carbonyl π-link provide an effective platform for electroluminescent materials, and their detailed electronic structure studies are useful for new molecular electronics device technology. The ground singlet state geometry optimizitation by density functional theory with the gradient and Hessian calculations made it possible to study IR spectra of thianthrene molecule and five benzoyl derivatives including series of fluoro-substituted isomers. Detailed comparison of all vibrational modes helped to carry out full assignments of the experimental FTIR spectra of newly synthesized compounds and solve structural problems associated with the X-ray diffraction analysis. It was shown that the change of fluorine atom position in the phenyl ring of benzoyl moiety leads to significant changes of dihedral angles and atomic charger distribution; this in turn leads to notable differences in dipole moments of these four isomers. As a result, in the IR spectra of fluoro-substituted isomers of benzoylthianthrene there are not only frequency shifts but also significant changes in the intensity of the corresponding IR bands. Although the experimental IR spectrum of thianthrene is well known, we have made its first ab initio assignment of all 60 vibrational modes. On this background, we explained the non-planar distortion of the thianthrene molecule in comparison with its planar ancestor — anthracene molecule, accounting vibronic activity of the b_{3u} vibrational mode (with imaginary frequency -i 67 cm^{-1}) of the D_{2h} point group. Knowledge of the accurate force field of all studied molecules made it possible to analyze the structure distortions of thianthrene in the ground and excited states and to transfer the similar vibronic perturbation theory to the benzoyl-containing derivatives accounting the pseudo-Jahn–Teller (PJT) effect.

Comparing the planar thianthrene configuration of the D_{2h} molecular symmetry, it was noted that the highest occupied molecular orbital b_{3u} becomes half-empty upon excitation to the S_1 and T_1 states. In the planar structure the S_1 state possesses the $^1B_{3g}$ symmetry ($b_{3u}\rightarrow a_u$ excitation). The pseudo-Jahn–Teller perturbing state along the puckering b_{3u} mode is the ^1A_u state produced by the $a_u\rightarrow a_g$ excitation. Such a state has a very high energy, and the distorting PJT effect in the S_1 excited thianthrene is strongly suppressed in comparison with the ground S_0 state. This vibronic analysis of the b_{3u} puckering distortion was supported here by TD DFT geometry optimization of the S_1 excited thianthrene, which showed obvious trend to planarization. At the same time the fully optimized S_1 and T_1 states lost their symmetry and exhibited some pseudo-in-plane distortion.

The Hirshfeld surface analysis indicated the weak CH…F, CH…S and CH…O intermolecular interactions as barely visible pale red spots in the d_{norm} surface of the **T3F** crystal. We used the dimeric approach to determine their influence on the IR spectrum of **T3F**. It was found that only CH…O intermolecular interactions appear in the IR spectrum of **T3F** crystal as two very weak stretching in-phase and stretching out-of-phase vibrations at 3084 and 3078 cm^{-1}, respectively.

Acknowledgements

This study was supported by the Ministry of Education and Science of Ukraine (projects no. 0122U000760), This project has also received funding from the Research Council of Lithuania (Project "ELOS" No S-MIP-21-7).

References

1 Arena, A., Campagna, S., Mezzasalma, M., Saija, R. & Saitta, G. (1993). Analysis of the Phosphorescence of Thianthren Crystals. *Nuovo Cimento*, *15*, 1521–1532. https://doi.org/10.1007/BF02451943

2 Pander, P., Swist, A., Soloducho, J. & Dias, F.B. (2017). Room temperature phosphorescence lifetime and spectrum tuning of substituted thianthrenes. *Dyes and Pigments*, *142*, 315–322. http://dx.doi.org/10.1016/j.dyepig.2017.03.049

3 Volyniuk, L., Gudeika, D., Panchenko, A., Minaev, B.F., Mahmoudi, M., Simokaitiene, J., Bucinskas, A., Volyniuk, D. & Grazulevicius J.V. (2023). Single-molecular white emission of organic thianthrene-based luminophores exhibiting efficient fluorescence and room temperature phosphorescence induced by halogen atoms. *ACS Sustainable Chemistry & Engineering* (in press).

4 Bersuker, I.B. (2013). Pseudo-Jahn–Teller Effect — A Two-State Paradigm in Formation, Deformation, and Transformation of Molecular Systems and Solids. *Chemical Review, 113*, 1351–1390. https://doi.org/10.1021/cr300279n

5 Gorinchoy, N.N. & Bersuker, I.B. (2017). Pseudo Jahn-Teller effect in control and rationalization of chemical transformations in two-dimensional compounds. *Journal of Physics: Conf. Series, 833*, 012010. https://doi.org/10.1088/1742-6596/833/1/012010

6 Becke, A.D. (1993). Density-functional thermochemistry. III. The role of exact exchange. *J. Chem. Phys., 7*, 5648–5652. https://doi.org/10.1063/1.464913

7 Lee, C., Yang, W. & Parr, R. G. (1988). Development of the Colle-Salvetti correlation-energy formula into a functional of the electron density. *Phys. Rev. B Condens. Matter*., *37*, 785–789. https://doi.org/10.1103/physrevb.37.785

8 Raghavachari, K., Binkley, J.S., Seeger, R. & Pople, J.A. (1980). Selfconsistent molecular orbital methods. 20. Basis set for correlated wave functions. *J. Chem. Phys*., *72*, 650–654. https://doi.org/10.1063/1.438955

9 Stewart, J.J.P. (1989). Optimization of parameters for semi-empirical methods I. Method. *J. Comput. Chem., 10*, 209–220. https://doi.org/10.1002/jcc.540100208

10 Stewart, J.J.P. (2004). Optimization of parameters for semi-empirical methods IV: extension of MNDO, AM1, and PM3 to more main group elements. *J. Mol. Model*., *10*, 155–164. https://doi.org/10.1007/s00894-004-0183-z

11 Cambridge Crystallographic Data Centre. (2023, May 15) CCDC deposition number 2160882. https://www.ccdc.cam.ac.uk/structures/Search? Ccdcid=2160882&DatabaseToSearch=Published

12 Scott, A. P. & Radom, L. (1996). Harmonic vibrational frequencies: an evaluation of Hartree−Fock, Møller−Plesset, quadratic configuration interaction, density functional theory, and Semiempirical scale factors. *J. Phys. Chem.*, *100*, 16502–16513. https://doi.org/10.1021/jp960976r

13 Dennington, R., Keith, T.A., Millam & J.M. (2016). GaussView, Version 6. Semichem Inc., Shawnee Mission, KS. https://gaussian.com/gaussview6/

14 Zhurko, G.A., Zhurko, G.A. & Romanov, A. (2011). Chemcraft — graphical software for visualization of quantum chemistry computations. http://www.chemcraftprog.com/

15 Frisch, M.J., Trucks, G.W., Schlegel, H.B., Scuseria, G.E., Robb, M.A., Cheeseman, J.R. et al. (2016). Gaussian 16, Revision A.03, Gaussian, Inc., Wallingford, CT. https://gaussian.com/

16 Turner, M.J., McKinnon, J.J., Wolff, S.K., Grimwood, D.J., Spackman, P.R., Jayatilaka, D. & Spackman, M.A. (2017). Crystal Explorer 17.5. University of Western Australia. https://crystalexplorer.net/

17 McKinnon, J.J., Spackman, M.A. & Mitchell, A.S. (2004). Novel tools for visualizing and exploring intermolecular interactions in molecular crystals. *Acta Crystallogr. Sect. B Struct. Sci., 60*, 627–668. https://doi.org/10.1107/S0108768104020300

18 Lynton, H. & Cox, E.G. (1956). The Crystal and Molecular Structure of Thianthren. *J. Chem. Soc.,* 4886–4895. https://doi.org/10.1039/JR9560004886

19 NIST Chemistry WebBook. (2023, May 15). Thianthrene. https://webbook.nist.gov/cgi/cbook.cgi? ID=C92853&Mask=80

20 Socrates, G. (2001). Infrared Raman Characteristic Group Frequencies — Tables and Charts, 3rd ed. J. Wiley&Sons, Chichester. https://doi.org/10.1021/ja0153520.

21 Minaeva, V.A., Karaush-Karmazin, N.N., Panchenko, A.A., Heleveria, D.N. & Minaev, B.F. (2021). Hirshfeld surfaces analysis and DFT study of the structure and IR spectrum of N-ethyl-2-amino-1-(4-chlorophenyl)propan-1-one (4-CEC) hydrochloride. *Comput. Theor. Chem.*, 1205, 113455. https://doi.org/10.1016/j.comptc.2021.113455

22 Minaeva, V., Panchenko, A., Karaush-Karmazin, N., Nycz, J. & Minaev, B. (2023). Manifestation of Intermolecular Interactions in the IR Spectra of 2- and 4-Methylmethcathinones Hydrochlorides: DFT Study and Hirshfeld Surfaces Analysis. *Biointerface Res. Appl. Chem.*, 13, 202. https://doi.org/10.33263/BRIAC133.202

23 Minaeva, V., Karaush-Karmazin, N., Panchenko, A., Minaev, B. & Ågren, H. (2023). Hirshfeld and AIM Analysis of the Methylone Hydrochloride Crystal Structure and Its Impact on the IR Spectrum Combined with DFT Study. *Crystals*, 13, 383. https://doi.org/10.3390/cryst13030383

Information about authors*

Minaeva, Valentina Alexandrovna — Senior Researcher, Assistant Professor, Department of Chemistry and Nanomaterials Science, Bohdan Khmelnytsky National University, 18031, Cherkasy, Ukraine; e-mail: minaeva@cdu.edu.ua; https://orcid.org/0000-0001-9318-1661

Karaush-Karmazin, Natalia Mikolaevna (*corresponding author*) — Senior Researcher, Department of Chemistry and Nanomaterials Science, Bohdan Khmelnytsky National University, 18031, Cherkasy, Ukraine; e-mail: karaush22@ukr.net; https://orcid.org/0000-0001-9360-2593

Panchenko, Olexandr Olexandrovich — Researcher, Department of Chemistry and Nanomaterials Science, Bohdan Khmelnytsky National University, 18031, Cherkasy, Ukraine; e-mail: panchenko9b@gmail.com; https://orcid.org/0000-0001-7669-1424

Chernyk, Maryana Vitalievna — Undergraduate, Department of Chemistry and Nanomaterials Science, Bohdan Khmelnytsky National University, 18031, Cherkasy, Ukraine; e-mail: maryana2001a@gmail.com;

Simokaitiene, Jurate — Dr., Department of Polymer Chemistry and Technology, Kaunas University of Technology Barsausko 59, LT-51423, Kaunas, Lithuania; e-mail: jurate.simokaitiene@ktu.lt, https://orcid.org/0000-0003-0657-4980

Volyniuk, Dmytro Yu. — Dr., Department of Polymer Chemistry and Technology, Kaunas University of Technology, Barsausko 59, LT-51423, Kaunas, Lithuania; e-mail: dmytro.volyniuk@ktu.lt; https://orcid.org/0000-0003-3526-2679

Grazulevicius, Juozas Vidas — Professor, Department of Polymer Chemistry and Technology, Kaunas University of Technology, Barsausko 59, LT-51423, Kaunas, Lithuania; e-mail: juozas.grazulevicius@ktu.lt; https://orcid.org/0000-0002-4408-9727

Minaev, Boris Filippovich (*corresponding author*) — Doctor Of Chemical Sciences, Professor, Department of Chemistry and Nanomaterials Science, Bohdan Khmelnytsky National University, 18031, Cherkasy, Ukraine; Senior Researcher, Department of Physics and Astronomy, Uppsala University, SE-752 37 Uppsala, Sweden; e-mail: bfmin43@ukr.net; https://orcid.org/0000-0002-9165-9649

Reshetnyak, Oleksandr Volodimirovich — Professor, Chairperson, Department of Physical and Colloid Chemistry, Ivan Franko National University of Lviv, Universitetskaya st., 1, 79000, Lviv, Ukraine; e-mail: oleksandr.reshetnyak@lnu.edu.ua; https://orcid.org/0000-0001-9669-9431

*The author's name is presented in the order: *Last Name, First and Middle Names*